Journal of
Mechanics of
Materials and Structures

EFFECTS OF IN-PLANE ELECTRIC FIELDS ON THE TOUGHENING BEHAVIOR OF FERROELECTRIC CERAMICS

Jianxin Wang and Chad M. Landis

Volume 1, Nº 6 June 2006

mathematical sciences publishers

JOURNAL OF MECHANICS OF MATERIALS AND STRUCTURES
Vol. 1, No. 6, 2006

EFFECTS OF IN-PLANE ELECTRIC FIELDS ON THE TOUGHENING BEHAVIOR OF FERROELECTRIC CERAMICS

JIANXIN WANG AND CHAD M. LANDIS

Mode-I steady state crack growth in poled ferroelectric ceramics subjected to simultaneous electrical and mechanical loading is analyzed to investigate the effect of in-plane electric fields and polarization on the toughening behavior. A multiaxial, incremental constitutive law for domain switching is implemented within the finite element method to obtain the electromechanical crack tip fields. Simulation results are presented for the cases of initial remanent polarization states and applied electric fields perpendicular to the crack plane and parallel to the crack growth direction. Specific results from the calculations include the shapes and sizes of switching zones, and the toughening effects due to domain switching near the crack tip.

1. Introduction

Ferroelectric ceramics have been widely used in smart structure applications due to their large electromechanical coupling effects. Since ferroelectric devices often operate under strong mechanical and electrical loading conditions, the brittle ferroelectric ceramic material is susceptible to fracture. Therefore, an understanding of ferroelectric fracture is a key issue for the efficient and reliable design of these devices. This paper is concerned with the study of the Mode-I fracture behavior of ferroelectric ceramics under combined in-plane electrical and mechanical loading.

The scenario investigated here is illustrated in Figure 1. A ferroelectric material is initially poled by an electric field either perpendicular or parallel to the direction of crack growth. After the initial poling, an electric field is applied along (positive electric field) or opposite (negative electric field) to the initial poling direction. Finally, mechanical loading is applied and crack growth occurs. Experimental observations of the fracture properties of ferroelectrics under such conditions have been obtained on several materials from indentation tests and compact tension specimens. Using indentation tests on a PZT-8 material composition, Tobin and Pak [1993] showed that for cracks perpendicular to the poling direction, the apparent fracture toughness decreases with positive electric field and increases with a negative field. For cracks parallel to the poling direction, their results indicated that both positive and negative electric fields have little influence on the toughening. Tobin and Pak [1993] also observed that with no applied electric field the fracture toughness was greater for cracks parallel to the poling direction than for cracks perpendicular to the poling direction. Park and Sun [1995] investigated electric field effects on crack growth in a PZT-4 ceramic by using conventional compact tension fracture tests. Their results agree with those of Tobin and Pak [1993] for the case of electric field applied perpendicular to the crack surface. However, the Vickers indentation tests of Wang and Singh [1997] showed that if the applied electric fields are perpendicular to the crack in a PZT EC-65 ceramic, then a positive electric field impedes

Keywords: fracture toughness, finite elements, ferroelectrics, piezoelectrics, domain switching.

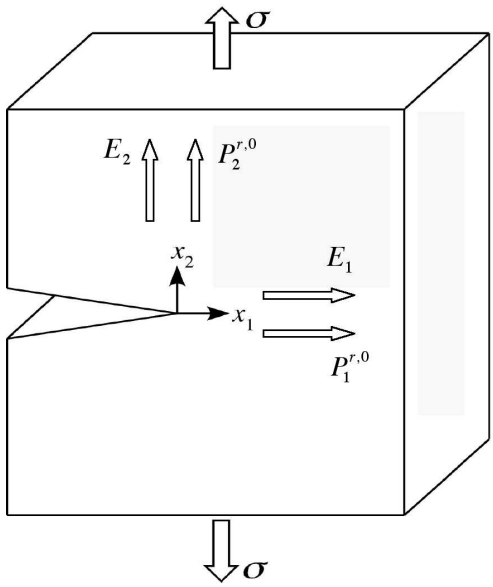

Figure 1. A schematic of the in-plane electrical and in-plane mechanical configuration to be modeled in this work. For any given sample, the electric field and remanent polarization are aligned in x_1 or x_2 direction. The in-plane mechanical loading is simply indicative of the Mode I symmetry to be modeled in this work and should not be interpreted literally.

crack propagation, whereas a negative electric field promotes crack propagation. For the electric field parallel to the crack, their results indicated that a negative field has little effect on the crack propagation while a positive field impedes crack propagation. Schneider and Heyer [1999] studied the effect of a static electric field on the fracture behavior of ferroelectric barium titanate using indentation tests. Their results indicate that the measured crack length versus the applied electric field shows hysteresis similar to the strain hysteresis. The more recent compact tension tests and indentation fracture tests on a PZT-841 ceramic, Fu and Zhang [2000], observed the reduction in the fracture toughness for a positive electric field as well as for a negative electric field if the electric field is applied perpendicular to the crack surface. Lucato et al. [2002] and Hackemann and Pfeiffer [2003] performed steady crack growth experiments and recorded R-curve behavior for a variety of electrical polarization conditions. It is the existence of this R-curve behavior that indicates that the toughness variations are at least influenced by an irreversible constitutive process occurring around the crack.

Several theoretical models have been proposed in an attempt to evaluate the effect of electric field on fracture toughness of ferroelectric ceramics. It is widely accepted that the nonlinear and hysteretic constitutive behavior of ferroelectrics plays a significant role in the fracture toughness behavior. Yang and Zhu [1998] and Beom and Atluri [2003] applied transformation toughening concepts to study the effects of electric field and domain switching on the fracture toughness. Zeng and Rajapakse [2001] considered the anisotropic material properties and electromechanical coupling effect of ferroelectric ceramics and showed that a positive electric field impedes the propagation of a crack perpendicular to the poling

direction while a negative field enhances it. In contrast to these approximate analytical models, this study applies an established constitutive model for the ferroelectric constitutive behavior within finite element computations to accurately determine the enhancement of the fracture toughness due to domain switching near a growing crack. More comprehensive reviews of the recent experimental and modeling efforts on ferroelectric fracture can be found in [Zhang et al. 2001] and [Chen and Lu 2002].

The purpose of this study is to investigate the effect of electric fields on fracture behavior of ferroelectric ceramics subjected to combined electrical and mechanical loading. The nonlinear phenomenological constitutive model for coupled electromechanical domain switching is presented in Section 2. In Section 3, the fracture model and the finite element formulation which implements the constitutive model for steady crack growth will be described. The results are presented and analyzed in Section 4. A discussion of the results and comparisons to experimental observations are included in Section 5.

2. The phenomenological constitutive model

The goal of any phenomenological constitutive theory is to provide a relatively simple framework within which the laws of thermodynamics are satisfied and a wide range of material behaviors can be represented. A summary of the recent developments on microelectromechanical and phenomenological constitutive modeling of ferroelectrics can be found in review articles by Kamlah [2001] and Landis [2004c]. The phenomenological constitutive model presented below is based on the work of Landis [2002a; 2003b; 2004]. This constitutive model has been verified against experimental observations and microelectromechanical self-consistent simulations based on the model of Huber et al. [1999]. A formulation of the model required to investigate the toughening behavior of the poled ferroelectric ceramics under different poling directions with in-plane mechanical loading only is presented here.

In this work, it is assumed that the mechanical loading is applied in the $x_1 - x_2$-plane and electric field is applied either in the x_1 or in x_2 direction as illustrated in Figure 1. Due to the constraint of plane-strain, axial stresses in the x_3 direction are allowed to develop as well. In a polycrystal, the linear elastic, dielectric and piezoelectric properties are dependent on the remanent strain and remanent polarization history at each material point. For a material poled by a uniaxial electric field these properties will be homogeneous and transversely isotropic about the poling direction. In comparison to the piezoelectric properties, which must change sign as the direction of the remanent polarization reverses, the elastic and dielectric properties have a much weaker dependence on the remanent state. Hence, for simplicity it will be assumed that elastic compliance at constant electric field, s^E_{ijkl}, and the dielectric permittivity at constant stress, κ^σ_{ij}, are not affected by changes in the remanent polarization of the material. The piezoelectric properties are assumed to be linearly dependent on the remanent polarization and transversely isotropic about the remanent polarization direction. Given these assumptions the s^E_{ijkl} and κ^σ_{ij} tensors will take on their isotropic forms. However, due to the presence of piezoelectricity and its dependence on the remanent polarization, other elastic and dielectric tensors such as the elastic stiffness at constant electric displacement, c^D_{ijkl}, and the inverse dielectric permittivity at constant strain, β^ε_{ij}, will have transversely isotropic symmetry about the remanent polarization direction. With these assumptions the constitutive

relationships can then be expressed as

$$\varepsilon_{ij} - \varepsilon^r_{ij} = \frac{1+v}{E}\,\sigma_{ij} - \frac{v}{E}\sigma_{kk}\delta_{ij} + d_{kij}E_k, \tag{2–1}$$

$$D_i - P^r_i = d_{ikl}\sigma_{kl} + \kappa E_i, \tag{2–2}$$

where

$$d_{kij} = \frac{d_{33}}{4}\frac{P^r}{P_0}\big(3n_i\delta_{jk} + 3n_j\delta_{ik} - 2n_k\delta_{ij}\big), \qquad P^r = \sqrt{P^r_i P^r_i}$$

$$n_i = P^r_i / P^r.$$

Here, ε_{ij}, ε^r_{ij}, D_i and P^r_i are the Cartesian components of the strain, remanent strain, electric displacement and remanent polarization, respectively, and are referenced from a thermally depolarized state. The components of the stress and electric field are σ_{ij} and E_i. The isotropic elastic properties are the Poisson's ratio v and the Young's modulus E, and δ_{ij} is the Kronecker delta. The dielectric permittivity is κ. Finally, d_{33} is the piezoelectric coefficient when P^r reaches the maximum attainable remanent polarization P_0, and n_i is a unit vector in the direction of the remanent polarization. Note that this form for the piezoelectric coefficients has $d_{31} = -d_{33}/2$ and $d_{15} = 3d_{33}/2$. This is a reasonable assumption based on measured values in polycrystals, and this assumption can be relaxed at the added expense of complexity within the theory.

The purpose of the nonlinear constitutive law is to provide the evolution of the stress, electric displacement, remanent strain and remanent polarization histories given the total strain and electric field histories. Domain switching occurs when a specific switching condition is met. This switching criterion can be used to define a surface in stress and electric field space and will be referred to as the switching surface. The specific form of the switching surface implemented here is that proposed by Landis [2002a]

$$\Phi = \frac{3\hat{s}_{ij}\hat{s}_{ij}}{2\sigma_0^2} + \frac{\hat{E}_i\hat{E}_i}{E_0^2} + \frac{\beta\hat{E}_i P^r_j \hat{s}_{ij}}{E_0 P_0 \sigma_0} - 1 = 0, \tag{2–3}$$

where

$$\hat{\sigma}_{ij} = \sigma_{ij} - \sigma^B_{ij}, \qquad \text{with } \hat{s}_{ij} = \hat{\sigma}_{ij} - \frac{1}{3}\sigma_{kk}\delta_{ij}$$

$$\hat{E}_i = E_i - E^B_i + \frac{\partial d_{jkl}}{\partial P^r_i}E_j\sigma_{kl}. \tag{2–4}$$

Here σ^B_{ij} is the back stress tensor, E^B_i is the back electric field, σ_0 is the initial switching strength of the material in uniaxial tension or compression, E_0 is the coercive field, and β is a positive scalar parameter. The postulate of maximum dissipation is satisfied if the switching surface is convex and the increments of remanent strain and polarization are normal to the surface. The switching surface defined in Equation (2–3) is convex if $\beta < 3$. Normality requires the remanent increments to be given as

$$\dot{\varepsilon}^r_{ij} = \lambda\frac{\partial\Phi}{\partial\hat{\sigma}_{ij}} \qquad \text{and} \qquad \dot{P}^r_i = \lambda\frac{\partial\Phi}{\partial\hat{E}_i}, \tag{2–5}$$

where λ is the switching multiplier. To determine the back stress and back electric field, it is assumed that the remanent strain and remanent polarization can be applied as internal variables that fully characterize the thermodynamic state of the material. This assumption leads to the identification of a remanent potential, $\Psi^r(\varepsilon^r_{ij}, P^r_i)$, such that the back stress and back electric field components can be derived from the potential in the following manner:

$$\sigma^B_{ij} = \frac{\partial \Psi^r}{\partial \varepsilon^r_{ij}}, \qquad E^B_i = \frac{\partial \Psi^r}{\partial P^r_i}. \tag{2–6}$$

Finally, the form of Ψ^r must be specified to complete the constitutive theory. For the results to be presented Ψ^r is split into a mechanical part Ψ^σ that enforces the strain saturation conditions, and an electrical part Ψ^E that enforces the polarization saturation conditions,

$$\Psi^r = \Psi^\sigma + \Psi^E \tag{2–7}$$

$$\Psi^\sigma = \frac{1}{2} H^\sigma_0 \varepsilon_c \left[\frac{J^e_2}{\varepsilon_c} \exp\left(\frac{m}{1 - \bar{\varepsilon}/\varepsilon_c} \right) \right]^2, \tag{2–8}$$

where H^σ_0 is a characteristic level of back stress that primarily affects the initial slope of uniaxial stress versus remanent strain curve, m is another hardening parameter that controls how abruptly the strain saturation conditions can be approached. The multiaxial remanent strain saturation conditions are enforced by causing Ψ^σ to approach infinity as the strain-like variable $\bar{\varepsilon}$ approaches the saturation level of remanent strain in uniaxial compression ε_c. The effective saturation remanent strain quantity $\bar{\varepsilon}$ is defined as

$$\bar{\varepsilon} = J^e_2 f\left(J^e_3/J^e_2\right), \tag{2–9}$$

where

$$f\left(\frac{J^e_3}{J^e_2}\right) = -0.0965\left(\frac{J^e_3}{J^e_2}\right)^3 + 0.01\left(\frac{J^e_3}{J^e_2}\right)^6 + 0.8935, \text{ for } \left(\frac{J^e_3}{J^e_2}\right) < 0 \tag{2–10}$$

and

$$f\left(\frac{J^e_3}{J^e_2}\right) = -0.1075\left(\frac{J^e_3}{J^e_2}\right)^3 - 0.027\left(\frac{J^e_3}{J^e_2}\right)^6 - 0.028\left(\frac{J^e_3}{J^e_2}\right)^{21} + 0.8935, \text{ for } \left(\frac{J^e_3}{J^e_2}\right) \geq 0. \tag{2–11}$$

Here, f is a functional fit to the numerical results obtained from the micromechanical computations described in [Huber et al. 1999]. The following remanent strain invariants are used to describe the multiaxial remanent strain state

$$J^e_2 = \left(\frac{2}{3} e^r_{ij} e^r_{ij}\right)^{1/2} \text{ and } J^e_3 = \left(\frac{4}{3} e^r_{ij} e^r_{jk} e^r_{ki}\right)^{1/3}, \tag{2–12}$$

where e^r_{ij} is the remanent strain deviator, $e^r_{ij} = \varepsilon^r_{ij} - \delta_{ij}\varepsilon^r_{kk}/3$.

Next, the electrical part of Ψ^r has the form of

$$\Psi^E = H^E_0 P_0 \left[\ln\left(\frac{1}{1 - P^r/P_{sat}} \right) - \frac{P^r}{P_{sat}} \right], \tag{2–13}$$

where

$$P_{sat} = \frac{3P_0}{4\left(\varepsilon_t + \varepsilon_c\right)}\left(\varepsilon^r_{ij} n_i n_j + \varepsilon_c\right) + \frac{P_0}{4}. \tag{2–14}$$

Here ε_t is the remanent saturation strain in uniaxial tension and, according to Equations (2–8)–(2–11), is equal to $1.368\varepsilon_c$. The maximum attainable remanent polarization P_0 has been defined previously. Note that the level where the remanent polarization saturates P_{sat} is a function of the remanent strain and the maximum of P_0 can only be attained if $\varepsilon^r_{ij} n_i n_j = \varepsilon_t$. If $\varepsilon^r_{ij} n_i n_j = -\varepsilon_c$ then the maximum level for P^r is only $P_0/4$. This result and the linear approximation to the functional form for P_{sat} given in Equation (2–14) are taken directly from the microelectromechanical computations described in [Landis et al. 2004]. A more detailed description of the model can be found in references [Landis 2002a; Landis 2003b; Landis et al. 2004]. For the numerical implementation of the constitutive model into the finite element model, a backward Euler integration routine was developed to solve the constitutive equations. The scheme is similar to that described in [Landis 2003a].

3. The fracture model and finite element formulation

3.1. ***The loading process.*** Note that the straight lines within the loops in Figures 2a and 2b represent linear unloading during the removal of the applied electric field, and those in 2c and 2d depict the initial behavior during depolarization by compressive stress from different *partially* poled states. After the initial poling step or lack of it, the electromechanical loading history for the specimen is as follows. Electric field is applied in the x_α direction, again in the absence of mechanical stress. If the applied electric field is of sufficient magnitude then poling of initially unpoled samples or a reversal of poling in initially poled samples may result. In any case, this step in the electrical loading procedure induces new states of strain and electric displacement, which will be called the initial strain ε^0_{ij} and initial electric displacement D^0_i. The final step in the loading process is to apply the in-plane mechanical loads while keeping the applied electric field fixed at the level attained in the previous step. Under plane-strain conditions, the out-of-plane axial strain ε_{33} is assumed to remain unchanged from its state after the electrical loading step, that is, $\varepsilon_{33} = \varepsilon^0_{33}$. Steady crack growth then occurs while the in-plane mechanical loads are applied.

3.2. ***Boundary conditions.*** In the study of electromechanical fracture, determination of the crack face boundary conditions remains an unresolved question. Thorough reviews of the literature can be found in [McMeeking 1999], [Zhang et al. 2001] and [Chen and Lu 2002]. A point of contention among differing modeling approaches is the crack face boundary condition for the so-called "insulating" crack problem. Herein, three approaches have received considerable attention: the impermeable crack model, the permeable, or "closed", crack model, and the "exact" boundary conditions. In this paper, the permeable boundary condition will be used. Landis [2004a] has shown that the permeable crack boundary conditions are a reasonable approximation when the electrical discharge strength of the medium within the crack is small (the permeable conditions are exact when the discharge strength is zero).

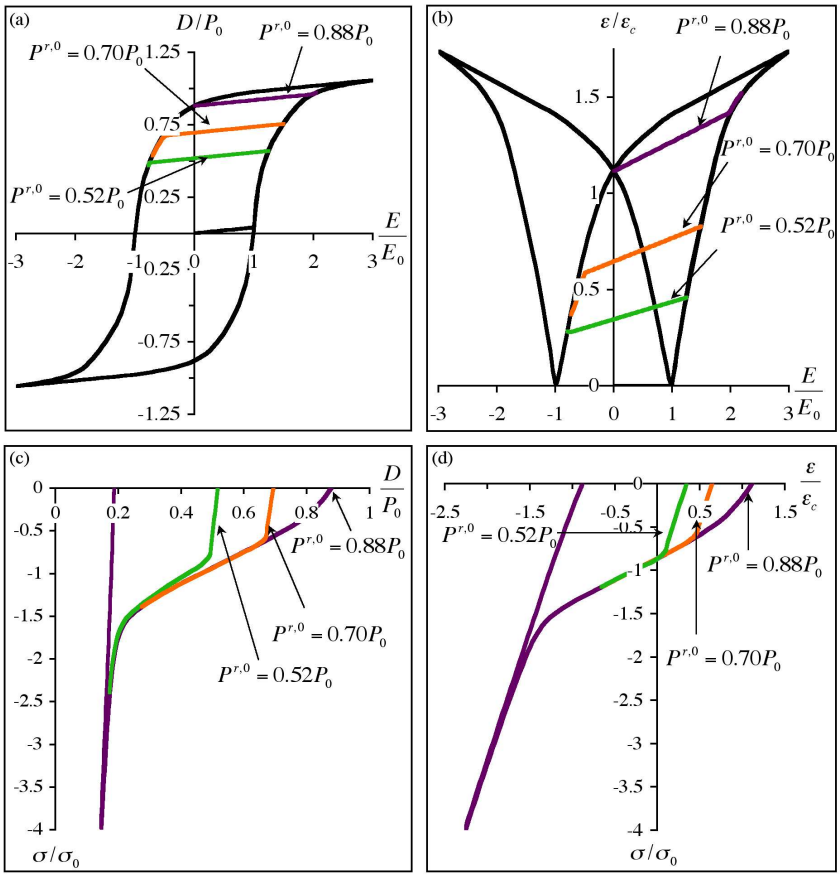

Figure 2. The uniaxial electromechanical behavior of the model material with three levels of the poling field, leading to different partially poled states: (a) the electric field versus electrical displacement hysteresis loops; (b) the electric field versus strain butterfly loop; (c) the stress versus electrical displacement depolarization loop; (d) the stress versus strain loop during depolarization. Notice that the intermediate lines in (a) and (b) represent the response during the unloading of electric field, and those in (c) and (d) represent the depolarization behavior from a partially poled state.

The electrically permeable and traction free crack face boundary conditions used in the present paper are stated as

$$D_2(r, \theta = \pi) = D_2(r, \theta = -\pi), \qquad \phi(r, \theta = \pi) = \phi(r, \theta = -\pi),$$
$$\sigma_{i2}(r, \theta = \pm\pi) = 0, \tag{3–1}$$

where ϕ is the electric potential, r and θ represent a polar coordinate system centered on the crack tip, and θ measures the angle between the radial direction and the x_1-axis. With a procedure similar to that outlined in [Landis 2004b], the asymptotic Mode I fields for the stresses and electric potential are

determined for the piezoelectric body and applied as far-field boundary conditions. The applied energy release rate for the far field is also determined from this solution. All of these quantities are not only dependent on K_I but also dependent on the piezoelectric coefficients, Young's modulus, Poisson's ratio, and initial remanent polarization $P_i^{r,0}$. Since the derivation is given in [Landis 2004b] and the results for the stresses involve relatively long formulas, only the applied energy release rate, G, is given here for brevity,

$$G = \begin{cases} -\dfrac{k_\varepsilon}{4D_D}\left(\dfrac{9D_E}{1+v} + 8(2-3\alpha_\varepsilon)\right)\dfrac{1-v^2}{E}K_I^2, & \text{poled parallel to the crack plane} \\ \dfrac{2k_\varepsilon\alpha_\varepsilon}{D_E}\dfrac{1-v^2}{E}K_I^2, & \text{poled perpendicular to the crack plane} \end{cases} \tag{3–2}$$

where

$$\begin{aligned} k_\varepsilon &= 2E(d_{31}P^{r,0})^2/P_0^2\kappa(1-v), \\ \alpha_\varepsilon &= \sqrt{1/(1-k_\varepsilon)}, \\ D_D &= k_\varepsilon(1-v) + 2(\alpha_\varepsilon - 1)(1+v), \\ D_E &= \kappa_\varepsilon\alpha_\varepsilon(1-v) + 2(\alpha_\varepsilon - 1)(1+v). \end{aligned}$$

3.3. ***Small scale switching.*** During crack growth, small scale switching will be assumed, such that the representative height of the nonlinear switching zone near the crack tip is much smaller than any other characteristic specimen dimension such as crack length, specimen width or ligament width. Furthermore, under plane-strain conditions it is assumed that the specimen thickness is much greater than the switching zone size as well. The assumption of small scale switching will not be valid when the switching occurs over the entire sample. However, it is assumed here that the in-plane applied mechanical loads can still be characterized by the applied energy release rate given by Equation (3–2). A characteristic length R_s can be identified as

$$R_s = \frac{1}{3\pi}\frac{GE'}{\sigma_0^2}. \tag{3–3}$$

Here E' is the plane strain Young's modulus and R_s is a reasonable measure of the half-height of the switching zone in an unpoled, mechanically loaded material.

The remaining nonlinear analysis presented in this paper will focus only on the toughening due to domain switching during the steady crack growth. Under steady growth conditions, all increments of field quantities can be related to derivatives with respect to the x_1 coordinate direction by

$$\dot{\chi} = -\dot{a}\frac{\partial\chi}{\partial x_1}. \tag{3–4}$$

Here, χ is any scalar field quantity such as a Cartesian component of remanent strain or remanent polarization. Since the constitutive model used in this study is rate independent, $\dot{a}$ represents the *increment* of crack advance in the x_1 direction. If rate dependent material behavior were considered then $\dot{a}$ would represent the crack growth *rate*, [Landis et al. 2000]. In either case, if inertial effects are neglected, the determination of the energy flux to the crack tip given by Equation (3–5) and the finite element

formulation to solve for the electromechanical fields derived from Equations (3–7) and (3–8) are the same. Only the integration of the constitutive law would change with the additional feature of rate dependence.

Within this model, crack propagation will be assumed to occur when the crack tip energy release rate G_{tip} reaches a critical value. In order to compute the relationship between the applied steady state energy release rate G_{ss} and G_{tip}, a steady state finite element formulation is implemented to determine the electromechanical fields. Then, under steady-state conditions, G_{tip} can be calculated using the electromechanical form of [Hutchingson 1974] I-integral as

$$G_{\text{tip}} = I \equiv \int_S \left(W n_1 - \sigma_{ij} n_j u_{i,1} + D_i n_i E_1\right) dS, \tag{3–5}$$

where S is a surface enclosing the crack tip, n_i are the components of the unit normal directed outward from the surface, u_i are the components of the displacement vector, D_i are the components of the electric displacement vector, E_1 is the electric field in x_1 direction, and W is the history dependent electric enthalpy density at a material point defined by

$$W = \int_0^{\varepsilon_{ij}, E_i} \sigma_{ij} d\varepsilon_{ij} - D_i dE_i \tag{3–6}$$

The calculation of G_{tip} is carried out after the finite element solution is obtained.

3.4. ***Finite element formulation.*** To compute the electromechanical fields numerically, the following finite element formulation is applied. If we assume that the free charge density in the volume is equal to zero, the vector potential formulation proposed by Landis [2002b] can be used. The finite element formulation required to solve the steady crack growth boundary value problem is based on the variational statement

$$\int_V \sigma_{ij} \delta\varepsilon_{ij} + E_i \delta D_i dV = \int_S t_i \delta u_i + \phi \delta\omega dS. \tag{3–7}$$

After the implementation of the constitutive law, Equation (3–7) becomes

$$\begin{aligned}
&\int_V \left(\left(c^{D,0}_{ijkl} \Delta\varepsilon^{n+1}_{kl} - h^0_{kij} \Delta D^{n+1}_k\right) \delta\Delta\varepsilon_{ij} + \left(-h^0_{ikl} \Delta\varepsilon^{n+1}_{kl} + \beta^{\varepsilon,0}_{ij} \Delta D^{n+1}_j\right) \delta\Delta D_i \right) dV \\
&\quad = \int_s \left(T_i \delta\Delta u_i + \phi \delta\Delta\omega\right) dS \\
&\qquad - \int_V \left(\left(\Delta c^D_{ijkl} \Delta\varepsilon^n_{kl} - \Delta h_{kij} \Delta D^n_k\right) \delta\Delta\varepsilon_{ij} + \left(-\Delta h_{ikl} \Delta\varepsilon^n_{kl} + \Delta\beta^{\varepsilon}_{ij} \Delta D^n_j\right) \delta\Delta D_i \right) dV \\
&\qquad + \int_V \left\{ \left(\left(c^{D,0}_{ijkl} + \Delta c^D_{ijkl}\right) \left(\varepsilon^{r,0}_{kl} + \Delta\varepsilon^{r,n}_{kl} - \varepsilon^0_{kl}\right) - \left(h^0_{kij} + \Delta h_{kil}\right) \left(P^{r,0}_k + \Delta P^{r,n}_k - D^0_k\right) \right) \delta\Delta\varepsilon_{ij} \right. \\
&\qquad \left. + \left(-\left(h^0_{ikl} + \Delta h_{ikl}\right) \left(\varepsilon^{r,0}_{kl} + \Delta\varepsilon^{r,n}_{kl} - \varepsilon^0_{kl}\right) + \left(\beta^{\varepsilon,0}_{ij} + \Delta\beta^{\varepsilon}_{ij}\right) \left(P^{r,0}_k + \Delta P^{r,n}_k - D^0_k\right) \right) \delta\Delta D_i \right\} dV,
\end{aligned} \tag{3–8}$$

where S is the boundary of the volume V, $\Delta\omega$ is the change of surface charge, $c^{D,0}_{ijkl}$, Δc^D_{ijkl} are the Cartesian components of the elastic stiffness tensor and its change due to the evolution of remanency, h^0_{kij} and Δh_{kij} are the third rank tensor of piezoelectricity and its change, and $\beta^{\varepsilon,0}_{ij}$ and $\Delta\beta^{\varepsilon}_{ij}$ are the second rank dielectric tensor and its change. $c^{D,0}_{ijkl}$, h^0_{kij} and $\beta^{\varepsilon,0}_{ij}$ are the material properties at the initial remanent

state and are functions of $P_i^{r,0}$, while Δc_{ijkl}^D, Δh_{kij}, and $\Delta \beta_{ij}^{\varepsilon}$ are the changes of the material properties due to the change of remanent polarization. The tractions acting on the boundary S are given as $t_i = \sigma_{ji} n_j$. These tractions and the electric potential on the outer boundary are determined with a procedure similar to [Landis 2004b] and the electrically permeable boundary conditions are applied as stated in Equation (3–1). Returning to the finite element formulation, after the application of the appropriate finite element interpolations and the cancellation of the appropriate variational terms, the left-hand side of Equation (3–8) represents the stiffness matrix dotted with the vector of unknown nodal displacements at the $n+1$th iteration. Note that this stiffness matrix depends on initial remanent polarization and this matrix remains constant for all iterations. The first integral on the right-hand side represents the vector of known applied nodal "forces" arising from the tractions due to the mechanical loading and electrical potential due to electrical loading, which correspond to a specified level of the far field applied energy release rate. Note that these applied "forces" do not change from iteration to iteration. The second term on the right-hand side is an integrated body force due to the changes in the material properties. Finally, the third term on the right-hand side can be viewed as the body force due to the distributions of remanent polarization and remanent strain in the material from the nth iteration. As alluded to in this discussion, the finite element Equation (3–8) is solved with an iterative technique. To begin, uniform remanent strain and polarization distributions are assumed, integrated on the right hand side of Equation (3–8), and added to the applied traction boundary conditions. Next, the system of finite element equations is solved to obtain a new but approximate solution for the nodal unknowns. A new approximate strain and electric displacement distribution is derived from these nodal unknowns. Then, the incremental constitutive model described in Section 2 is integrated along streamlines of constant height above the crack plane from $x = +\infty$ to $x = -\infty$ to obtain updated approximations for the stress, electric field, remanent strain, and remanent polarization distributions. The new remanent strain and remanent polarization distributions are then integrated on the right hand side of Equation (3–8) and the matrix solution/streamline integration procedure is repeated until a suitable level of convergence is achieved. Additional descriptions of the steady state crack growth finite element formulation can be found in [Landis 2003a]. Once convergence is obtained, the crack tip energy release rate is computed from Equation (3–5) using an electromechanical generalization of the domain integral technique of [Li et al. 1985].

4. Results

The goal of this paper is to investigate the influence of the electric field on the fracture behavior of ferroelectric materials when the electric field or the poling direction is applied parallel or perpendicular to the crack surface in the plane of crack growth. As outlined in Section 3.1, two cases of electrical loading will be considered here, the initially unpoled and initially poled cases. After electrical loading of either case, the electric field E_α, $(\alpha = 1, 2)$, is kept constant and the initial state ε_{ij}^0, $\varepsilon_{ij}^{r,0}$, D_i^0 and $P_i^{r,0}$ is attained for the fracture simulation, after which the mechanical load is applied. In order to identify important parameters that affect the toughness of ferroelectric materials a dimensional analysis is performed on the constitutive equations (2–1)–(2–14), and the fundamental differential field equations. Such analysis identifies the following normalized field variables, σ_{ij}/σ_0, $\varepsilon_{ij}/\varepsilon_c$, $\varepsilon_{ij}^r/\varepsilon_c$, D_i/P_0, P_i^r/P_0 and E_i/E_0. Each of these normalized field variables is a function of the normalized spatial coordinates x_1/R_s and x_2/R_s, and also depends on the initial remanent polarization $P_i^{r,0}/P_0$, the applied electric field

E_i^A/E_0, and normalized material parameters $E\varepsilon_c/\sigma_0$, $d_{33}E_0/\varepsilon_c$, $\kappa E_0/P_0$, $\sigma_0\varepsilon_c/E_0P_0$, H_0^σ/σ_0, H_0^E/E_0, ν, β and m. Finally, the normalized steady state toughness of the material G_{ss}/G_0 is not a spatially varying field and hence will only depend on the normalized material parameters. It would be a sizeable task to parametrically investigate the effects of all ten dimensionless material quantities identified here. Instead, this work will focus on the effects of the initial remanent polarization $P_i^{r,0}/P_0$ on the toughening for a specific set of material properties. These material properties and constitutive parameters are characteristic of a soft PLZT material as measured by Lynch [1996], and are specifically given as:

$$\begin{aligned} \sigma_0 &= 27.5 \text{ MPa}, & E_0 &= 0.35\,\text{MV/m}, \\ P_0 &= 0.26 \text{ C/m}^2, & \varepsilon_c &= 0.12\%, \\ \beta &= 2.95, & \kappa &= 6\times10^{-8}\,\text{C/m}\cdot\text{V}, \\ E &= 70 \text{ GPa}, & \nu &= 0.4, \\ d_{33} &= 3\times10^{-10}\text{ m/V}, & d_{31} &= -d_{33}/2, \\ m &= 0.01, & H_0^\sigma &= 0.5\sigma_0, \\ & & H_0^E &= 0.05E_0. \end{aligned}$$

It should be noted here that simply changing the parameters listed above does not always result in a model material that produces reasonable constitutive response like that displayed in Figure 2. Hence, if another material composition is to be modeled, it is likely that in addition to changing the constitutive parameters listed above, the functional forms of the remanent potentials of Equations (2–7), (2–8) and (2–13) must be changed as well.

4.1. ***Switching zones.*** As mentioned previously, the primary result of interest from each steady crack growth calculation is the ratio of the far field applied energy release rate, G_{ss}, to the crack tip energy release rate G_{tip}. However, prior to presenting results for the relative level of toughening, some features of the switching zones near the crack tip will be given first. Figure 3 illustrates the sizes and shapes of the switching zones around steadily growing cracks in initially unpoled material (a), and initially poled material (b, c, d, e). The specific electrical loading parameters used to generate these results are: (a) unpoled $P_\alpha^{r,0}/P_0 = 0$, $E_\alpha^A/E_0 = 0$, $(\alpha = 1, 2)$; (b) poled parallel to the crack $P_1^{r,0}/P_0 = 0.75$ with no applied field $E_1^A/E_0 = 0$; (c) poled perpendicular to the crack $P_2^{r,0}/P_0 = 0.75$ with no applied field $E_2^A/E_0 = 0$; (d) poled parallel to the crack $P_1^{r,0}/P_0 = 0.47$ with negative applied field $E_1^A/E_0 = -0.2$; and (e) poled perpendicular to the crack $P_2^{r,0}/P_0 = 0.47$ with negative applied field $E_2^A/E_0 = -0.2$. Note that the spatial coordinates have been normalized by the length scale $R_0 = G_0E'/3\pi\sigma_0^2$, which can be interpreted as the size of the switching zone in a mechanically loaded unpoled material when the applied energy release rate is equal to G_0. This normalization is used instead of R_s in order to make the scales on each plot in Figure 3 comparable.

In Figures 3a–e, the outer solid black line delineates the boundary between material that is undergoing changes in remanency due to the in-plane mechanical loading and material that is not. The inner solid red contour delineates the location inside the switching zone where the change in remanent strain reaches the characteristic elastic level of $\Delta\bar{\varepsilon}^r = \sigma_0/E$, and the inner solid blue contour is where the remanent polarization change achieves the characteristic linear dielectric level $|\Delta P^r| = \kappa E_0$. It is worth noting

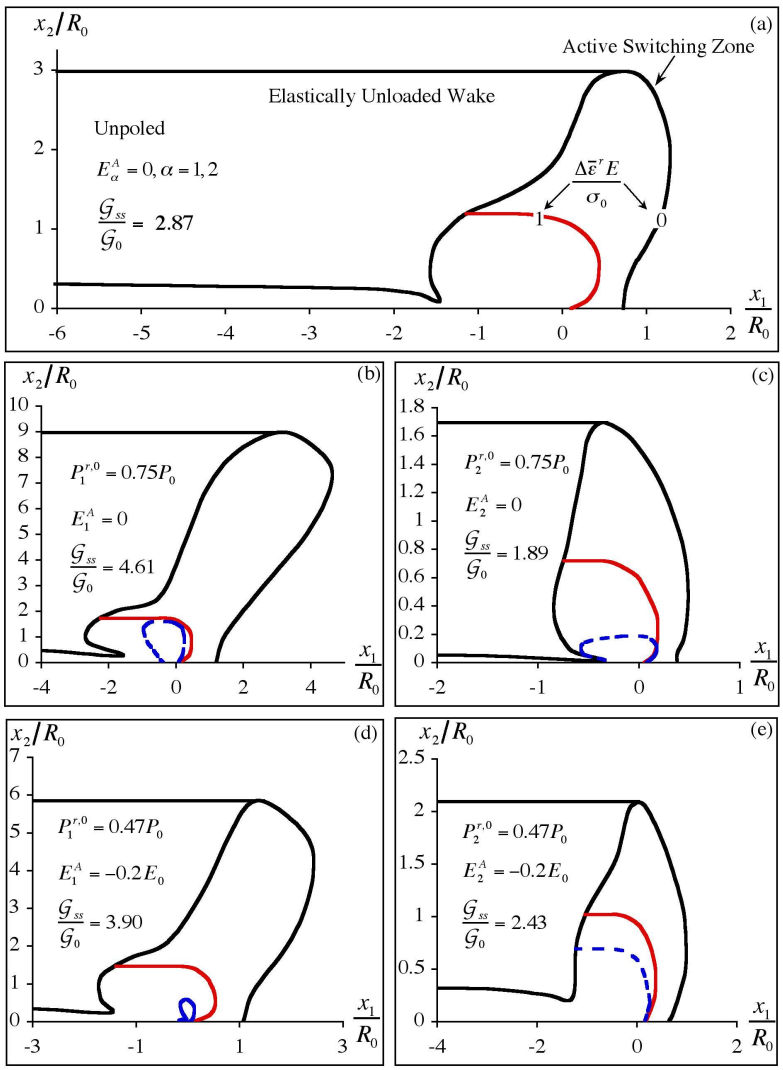

Figure 3. Switching zone sizes and shapes for initially unpoled (a) and initially poled (b)–(e) cases. The outermost curved contours on these plots delineate the location of the active switching boundary. The inner solid contours give the location within the active switching zones where the effective remanent strain change achieves the characteristic elastic level of $\Delta\bar{\varepsilon}^r \equiv \sqrt{2\Delta\varepsilon^r_{ij}\Delta\varepsilon^r_{ij}/3} = \sigma_0/E$. The inner dashed contours give the location within the active switching zones where the change of remanent polarization achieves the characteristic linear dielectric level $|\Delta P^r| = \kappa E_0$. Notice that the spatial coordinates are normalized by R_0, which is the characteristic switching zone size when the applied energy release rate reaches G_0, specifically, $R_0 = G_0 E'/3\pi\sigma_0^2$. Therefore, if G_0 is the same for all cases, then the spatial coordinate normalizations for each plot are identical.

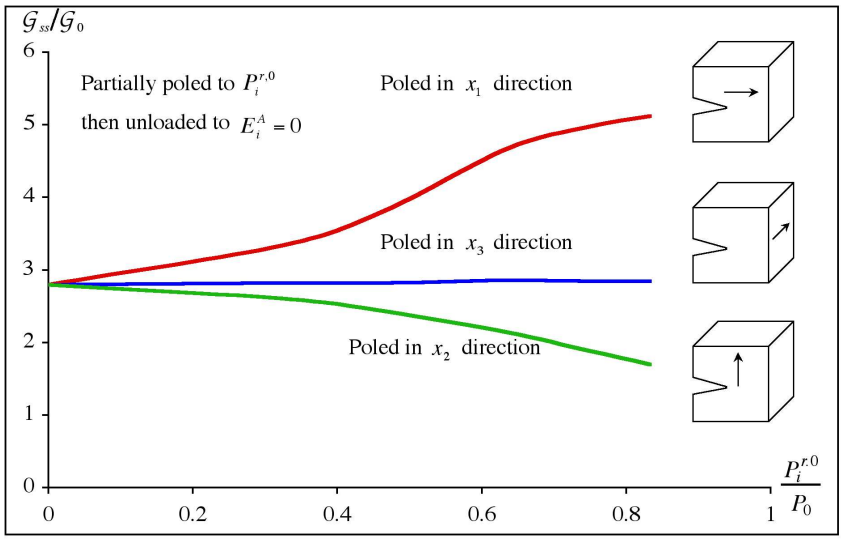

Figure 4. A comparison of the effects of poling direction on the toughness enhancement of partially poled materials. The normalized toughness enhancement G_{ss}/G_0 is plotted versus the initial remanent polarization state $P_i^{r,0}/P_0$, $i = 1, 2, 3$.

that in most cases the sizes of these inner switching zone contours where the effective remanent strain and polarization changes are equal to their characteristic linear values is significantly smaller than the outer switching zone boundary. This illustrates the fact that intense switching is confined to a region very close to the crack tip. Furthermore, note that the shapes of the switching zones depicted in these figures are that of the active switching zone. In other words, in the active switching zone, neighboring points at the same height above the crack plane have different remanent strain and polarization states. Whereas, in the linearly unloaded wake, neighboring points at the same height above the crack plane have identical remanent states. Lastly, material points outside of the active switching zone or the unloaded wake have a remanent state that is identical to that when the mechanical loading is initially applied.

4.2. ***The effect of initial electrical polarization on toughening.*** Within this model it is assumed that crack growth occurs when G_{tip} reaches the intrinsic fracture toughness of the material G_0. Hence the ratio G_{ss}/G_0 indicates the amount of toughening due to domain switching, with $G_{ss}/G_0 = 1$ corresponding to no toughness enhancement or R-curve behavior. With regard to R-curve behavior, G_0 should be interpreted as the applied energy release rate where crack growth first begins, and G_{ss} is the steady state or plateau level of the applied energy release rate after sufficiently large amounts of crack growth. Figure 4 shows the ratio of G_{ss}/G_0 versus the level of the initial remanent polarization under plane strain conditions. Electric field is first applied to pole the material to a given level and then removed. Thereafter, no electric field is applied. The cases for the material poled in the x_3 direction are taken from [Wang and Landis 2004] for comparison to the in-plane cases.

Prior to discussing the results for the initially poled cases, it is informative to construct a reasonable hypothesis for the qualitative behavior of the relative toughening, taking the toughening in the unpoled case as a reference. Since crack tips tend to cause higher stresses in the x_2 direction (for most polar

angles around the tip) it is reasonable to assume that the material's propensity for remanent straining in the x_2 direction will lead to greater toughening. For example, when a material is poled by an electric field in the x_1 direction, domains switch from being aligned closely to the x_2 and x_3 direction to the x_1 direction. Then, when a crack tip passes through with an accompanying large σ_{yy} component, the domains can switch back to the x_2 direction causing dissipation and toughening. In contrast, a material poled by an electric field in the x_2 direction will have most domains initially aligned closely with the x_2 direction. When a crack tip passes, nearby domains cannot switch again towards the x_2-axis and hence the dissipation due to domain switching will be relatively small. Applying these considerations, one would expect the following qualitative behaviors of the toughening: toughening should increase as the polarization in the x_1 or x_3 direction increases, and toughening should decrease as the polarization in the x_2 direction increases.

Figure 4 illustrates that as the initial remanent polarization increases the toughening, G_{ss}/G_0, will increase for poling parallel to the crack surface (x_1), decrease for poling perpendicular to the crack surface (x_2), and have little effect for poling parallel to the crack front (x_3). Hence, the qualitative hypotheses on toughening were correct for the x_1 and x_2 poling cases but incorrect for the x_3 case. It has been shown by Wang and Landis [2004], that the relatively weak dependence of the toughening ratio on the level of poling in the x_3 direction can be explained by considering the out-of-plane constraint imposed by the plane strain conditions. The qualitative explanation is as follows. If domains were to switch completely from being oriented towards the x_3 direction to an in-plane direction then this would cause a large negative remanent strain component ε^r_{33}. In order to maintain a total out-of-plane strain of zero, the elastic strain must then be positive and have the same magnitude as ε^r_{33}. This elastic strain component must arise from an out-of-plane stress component of a magnitude approximately equal to $E\varepsilon^r_{33}$. Therefore, if $|\varepsilon^r_{33}| > \sigma_0/E$, then the out-of-plane stress will be close to σ_0 and there will be a tendency for the domains to switch *back* towards the out-of-plane direction. The actual events do not proceed by switching in-plane and then switching back out-of-plane, but rather by switching only a relatively small amount. Hence, the out-of-plane constraint will negate the expected toughening effect described previously. This behavior has been verified experimentally by Hackemann and Pfeiffer [2003] who observed that samples poled parallel to the crack front had practically identical toughening to unpoled samples.

4.3. ***Effect of applied electric field on toughening: the perpendicular case.*** In this section, the results for the case when the electric field is applied perpendicular to the crack surface (in the x_2 direction) will be discussed in detail. Figure 5 shows the ratio of G_{ss}/G_0 versus the applied electric field in the x_2 direction for a range of initial poling states. The cases associated with the solid red and blue curves will be discussed first, as these cases essentially envelop the others and form an inverted butterfly loop. The red and blue regions of the inserted hysteresis and butterfly loops in the upper left and right hand corners correspond to the red and blue portions of the inverted toughness butterfly loop.

The results for fracture toughening can be explained qualitatively by considering the competing or complementary effects of the applied electric field and stress on domain switching near the crack tip. In general it is valid to assume that the crack tip stress field will tend to elongate the material in the x_2 direction and will tend to cause domain switching that will produce such an elongation. First, consider a thermally depolarized material poled by a strong uniaxial electric field in the x_2 direction. The states of

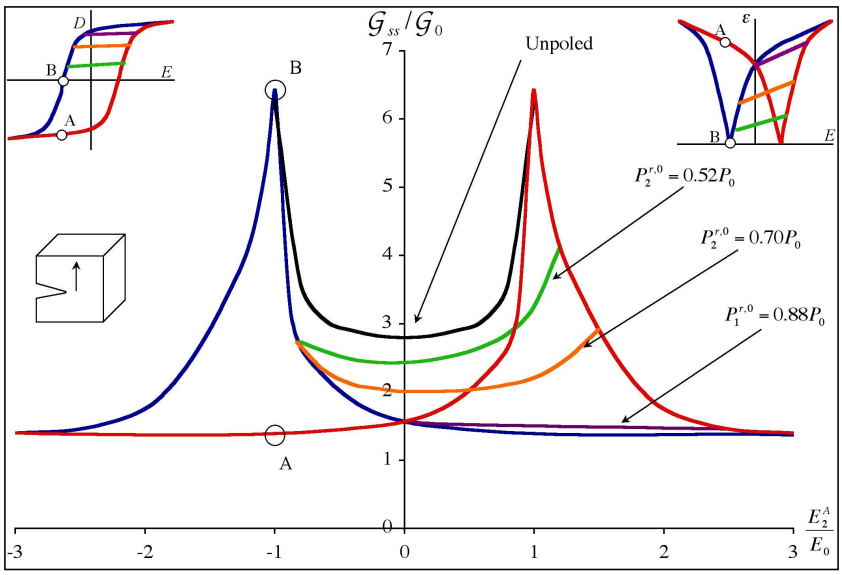

Figure 5. The normalized toughness enhancement G_{ss}/G_0 versus the applied electric field E_2 for a range of initial poling states for plane-strain conditions. The colored lines on the main plot correspond to the colored lines on the hysteresis and butterfly loops depicted in the inserts at the upper left and right corners. Points A and B are highlighted to indicate the relationships between the electromechanical constitutive response and the fracture toughness predictions.

electric displacement and strain for this material can be found at the upper right corners of the hysteresis loops in Figures 2a and 2b while the field is applied. If this level of applied electric field is held fixed at $3E_0$, steady crack growth occurs at an applied energy release rate of $G_{ss} = 1.4G_0$. This level of toughening is the lowest depicted on Figure 5. However, if the applied electric field was even greater, then the steady state toughness would continue to decrease, approaching G_0 as $E_2 \to \infty$. The qualitative reason for this behavior is that both the applied electric field and the stresses near the crack tip tend to cause domain switching towards the x_2 direction. If the initially applied electric field is sufficiently high, then almost all of the domains that can switch towards the x_2 direction will have done so prior to the growth of the crack. Thereafter, due to the lack of "switchable" domains, the mechanical loads cannot cause any additional switching and it is as if the crack is running through a linear, nondissipative, piezoelectric material. Since it is the domain switching process that gives rise to the dissipation of energy and the increase in fracture toughness, any phenomenon that inhibits any additional switching during crack growth, will also tend to decrease the fracture toughness. In contrast, applied electric field and initial poling states that allow the crack tip fields to cause additional switching will enhance the fracture toughening.

The remainder of the blue portion of the curve is obtained by first poling the material with a strong electric field, then reversing the electric field to a lower or negative applied electric field level of E_2^A, and finally applying the in-plane mechanical loading to produce steady crack growth. During this type

of initial electrical loading the electric displacement and strain behavior of the material traces out the outmost hysteresis loops depicted in Figures 2a and 2b and in the inserted plots in the upper left and right hand corners of Figure 5. As the electric field is removed, the inhibiting effect of the field on domain switching decreases and hence the fracture toughness increases. For positive levels of E_2^A, since most domains remain aligned in the x_2 direction, the increase in toughening remains small. However, when the applied electric field is reversed, some domains will switch towards the x_1 direction. Then, when the crack passes by, the crack tip fields will switch these domains back towards the x_2 direction creating both dissipation and fracture toughening. The most dramatic increase in the toughening occurs very close to $E_2^A = -E_0$, where reverse domain switching due to the applied electric field peaks. In fact, the spikes or "butterfly legs" of the toughness versus electric field curve in Figure 5 correspond to the legs of the butterfly loops in Figure 2b and the steep regions of the hysteresis loop in Figure 2a.

If the reversal of the initial applied electric field is large enough, that is, for $E_2^A < -E_0$, then the initial polarization of the material will be reversed as well, and the case where the remanent polarization and electric field are aligned is revisited. Hence, as the initial electric field is driven to large negative levels, it will again align domains in the x_2 direction, leaving little potential for switching due to the crack tip fields, which in turn causes low values of the steady state fracture toughening. Finally, the red curve is a mirror image of the blue curve and is obtained by poling in the negative x_2 direction first. Notice that points A and B are denoted on the three loops in this figure in order to aid in the understanding of the correlation between the fundamental electromechanical constitutive behavior and the fracture toughening predictions.

Also plotted Figure 5 are the cases where the material is partially poled by a moderate electric field, then the electric field is removed, a new electric field E_2^A is applied, and finally steady crack growth proceeds due to in-plane mechanical loading. For all of the partially poled cases negative E_2^A levels have similar trends with the fully poled, bold dashed curve described above. The differences between the partially poled cases and the fully poled cases are evident at intermediate levels of E_2^A. These levels of E_2^A correspond to the linear unloading regions indicated with the arrows on Figures 2a and 2b. At the same level of E_2^A, the toughening decreases with increasing initial remanent polarization if $-E_0 < E_2^A < E_0$. For large levels of E_2^A the partially poled cases eventually merge with the outer red and blue curves that represent the situations where the material has been initially poled by a strong electric field. The regions of similar toughening behavior between the partially and fully poled cases can be understood by considering the hysteresis and butterfly loops of Figure 2a and 2b. Specifically, the levels of applied electric field where the toughness curves merge in Figure 5 coincide with the electric field levels where the linear unloading segments for the partially poled materials meet the outer hysteresis and butterfly loops in Figure 2. At these levels of electric field, the partially poled materials commence additional nonlinear behavior.

4.4. ***Effect of applied electric field on toughening: parallel case.*** Figure 6 shows the ratio of G_{ss}/G_0 versus the applied electric field in x_1 direction for a range of initial poling states. Again, the cases associated with the red and blue curves will be discussed first. The read and blue regions of the inserted hysteresis and butterfly loops in the upper left and right hand corners correspond to the red and blue portions of the toughness butterfly loop. The similarities and differences between the perpendicular and parallel electrical loading cases will be explained in the following discussion.

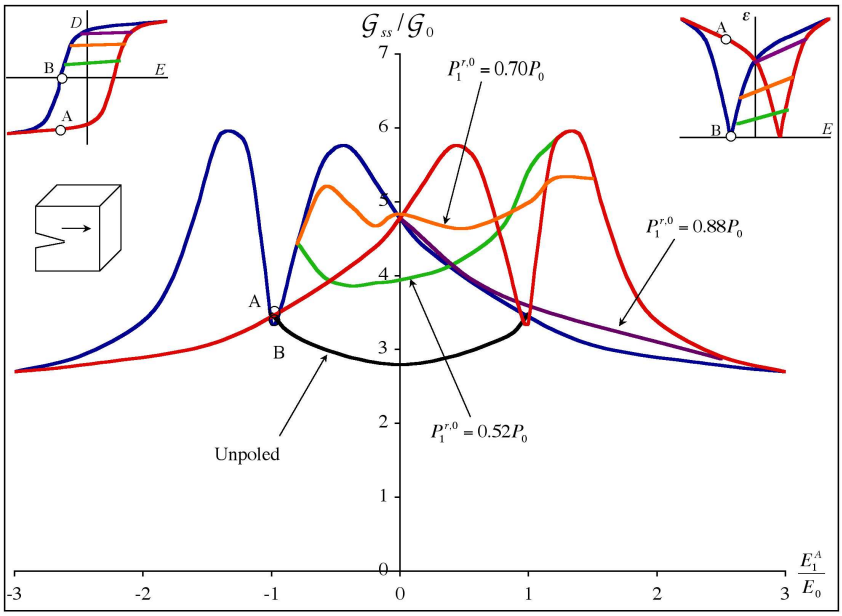

Figure 6. The normalized toughness enhancement G_{ss}/G_0 versus the applied electric field E_1 for a range of initial poling states for plane-strain conditions. The colored lines on the main plot correspond to the colored lines on the hysteresis and butterfly loops depicted on the inserts in the upper left and right corners. Points A and B are highlighted to indicate the relationships between the electromechanical constitutive response and the fracture toughness predictions.

First, consider a material poled by a strong uniaxial electric field of magnitude in the x_1 direction. As for the perpendicular poling case, if the applied electric field is sufficiently strong, it will be able to impede domain switching with the result that the fracture toughening is small. The primary difference between the parallel and perpendicular cases for this strong electrical loading scenario is that for the parallel case there will always be domains available to switch towards the x_2 direction. Then, unless the applied electric field E_1^A is extraordinarily strong, the singular crack tip fields will be able to switch domains towards the x_2 direction creating some toughness enhancement. In fact, for an applied electric field level of $E_\alpha^A = 3E_0$ the simulations predict that crack growth occurs at an applied energy release rate of $G_{ss} = 2.7G_0$ for applied field in the x_1 direction as compared to $G_{ss} = 1.4G_0$ for applied field in the x_2 direction. To summarize, the primary reason why toughening is low for strong electric fields applied perpendicular to the crack is that there is a dearth of domains available for switching towards the x_2 direction. Whereas for strong fields in the x_1 direction, domains are available for switching but the electric field prevents the domain switching towards the x_2 direction. In either case, the fracture toughening decreases as the applied electric field continues to increase.

Next consider the region of the blue curve on Figure 6 for the region $0 \leq E_1^A < 3E_0$. This region of the curve is obtained by first poling the material with a strong electric field, then partially removing the field to a lower level of E_1^A. Thereafter, the in-plane mechanical loading is applied to produce steady

crack growth. As the electric field is removed, the inhibiting effects of the electric field on domain switching towards the x_2 direction decreases and the fracture toughening increases. The region of the blue toughening curve with $0 \leq E_1^A < 3E_0$ can be relatively well understood because the initial polarization state is similar for all cases within this range and only the tendency for the applied electric field to align the polarization (and hence the strain) in the x_1 direction needs to be considered. In contrast, a qualitative description of the behavior in the range of $-1.4E_0 < E_1^A < 0$ is considerably more difficult to construct due to the competing effects of differing potential for change in axial strain in the x_2 direction and the tendency for the applied electric field to align the polarization in the x_1 direction. The model results for the specific material properties applied in the simulations indicate that the toughening increases in the range $-0.5E_0 < E_1^A < 0$, decreases for $-E_0 < E_1^A < -0.5E_0$, increases again for $-1.4E_0 < E_1^A < -E_0$, and finally decreases when $E_1^A < -1.4E_0$. First note that as the applied electric field traverses the range from $E_1^A = 0$ to $E_1^A = -E_0$ the remanent strain in the x_1 direction goes from approximately $\varepsilon_{11}^r = 1.1\varepsilon_c$ to $\varepsilon_{11}^r = 0$. Therefore, the case with the greatest potential for remanent straining towards the x_2 direction is at $E_1^A = 0$ and decreases until $E_1^A = -E_0$. Thereafter, the possible change of remanent strain towards the x_2 direction increases again as $E_1^A \to -\infty$. Hence, the toughening due to the potential remanent strain contribution should take the same shape as the strain-electric field butterfly loop. The fact that the x_1 toughening curve does not take this shape is due to the competing effect of the applied electric field tending to align the strain in the x_1 direction. The strength of this competing "force" is best quantified by the energetic term $E_1^A P_1^{r,0}$. In the range from $-E_0 < E_1^A < 0$, this quantity will actually be negative suggesting that the applied electric field "helps" the strain reorient towards the x_2 direction. At $E_1^A = 0$ this quantity will obviously be zero and at $E_1^A = -E_0$ this quantity will also be close to zero due to the fact that $P_1^{r,0} \approx 0$ when $E_1^A = -E_0$. For $E_1^A < -E_0$, both E_1^A and $P_1^{r,0}$ will be less than zero causing $E_1^A P_1^{r,0}$ to be positive indicating that these levels of applied electric field inhibit the toughening. Then, when the competing effects of potential strain and applied electric field are added together, an oversimplified but qualitatively valid understanding of the toughening curve of Figure 6 is obtained. Instead of the butterfly shaped toughening loop that would be expected if only the potential for remanent straining in the x_2 direction governed the behavior, the quantitative results predict that the effects of the applied electric field "fold" the butterfly loop "in half". Specifically, the tips of the "wings" at high applied electric field are inverted, but the "legs" remain in the same orientation.

Also shown on Figure 6 are the cases where the material is initially unpoled or partially poled by a moderate electric field, the electric field is removed, a new electric field E_1^A is applied, and finally steady crack growth proceeds due to in-plane mechanical loading. Of special interest is the behavior of the material near zero electric field for partial poling levels of $P_1^{r,0} = 0.52P_0$ and $P_1^{r,0} = 0.7P_0$. Note that the toughening trend near zero electric field for $P_1^{r,0} = 0.52P_0$ increases with applied electric field, whereas the trend is the opposite for a fully poled material. Also, the toughening behavior is relatively flat for the partial poling case of $P_1^{r,0} = 0.7P_0$. These intermediate poling cases illustrate the sensitivity of the toughening behavior to the initial polarization state of the material for crack growth along the applied electric field direction. Furthermore, it is our opinion that modest changes in the shapes of the hysteresis and butterfly loops of the material will also have a significant effect on the shape of the x_1 toughening curve. Specifically, changes in the material behavior will likely cause a shift in the location of the "fold" in the x_1 toughening curve.

5. Discussion

The model presented here differs from previous theoretical explanations of the effects of electric field and polarization on the fracture toughness of ferroelectrics in that an incremental, microelectromechanically tested, phenomenological constitutive law has been applied instead of a discrete switching law. Additionally, in contrast to applying simplifying assumptions associated with most transformation toughening models, the details of the electromechanical fields have been obtained from finite element computations. The fields computed in this work include both the perturbing influences of ferroelectric switching and the change of the piezoelectric effect that results from such switching. The detailed constitutive model applied in this work has allowed for both qualitative and quantitative characterizations of the effects of electric field on the toughening due to domain switching in ferroelectric ceramics. The model predicts a range of phenomena that indicate that the toughening is dependent on both the level of electric field, its direction of application, and on the initial polarization state.

The predictions of the present model are in qualitative accord with several different experimental observations. First, the model predictions displayed in Figure 4 indicate that the toughening is greater for crack growth parallel to the poling direction than for crack growth perpendicular to the poling direction for the in-plane cases. This prediction is in agreement with the observations of Tobin and Pak [1993] and Lucato et al. [2002]. When the polarization is parallel to the crack front, then the model predicts that there is little to no variation in the toughness with changes in the polarization. Again, this prediction is in agreement with the experimental observations of Hackemann and Pfeiffer [2003]. Additionally, the model results illustrated in Figure 3 indicate that domain switching is intense near the tip of the crack but diffuse towards the outer boundary of the switching zone. This prediction is also in agreement with the observations of Hackemann and Pfeiffer [2003]. Lastly, the model predictions shown in Figure 5, indicating that a positive electric field reduces toughening and negative electric field increases toughening for polarization perpendicular to the crack, are in agreement with the observations of both Tobin and Pak [1993] and Park and Sun [1995].

As discussed above, the present model is able to explain the experimental results observed by Hackemann and Pfeiffer [2003]. However, previous modeling efforts on the fracture toughness of ferroelectrics are not able to predict or explain such observations. Specifically, the simple model applied to analyze transformation toughening for partially stabilized zirconia [McMeeking and Evans 1982] has been used to determine switching zones and fracture toughening during crack growth in ferroelectrics. These models assume that once a specific switching criterion is met, for example,

$$E_i \Delta P_i^r + \sigma_{ij} \Delta \varepsilon_{ij}^r = G_c,$$

[Hwang and McMeeking 1998] the material attains a finite transformation polarization ΔP_i^r and strain $\Delta \varepsilon_{ij}^r$ that remains fixed and frozen into the material. This is in contrast to the incremental flow rule used in the present model that allows both the polarization and strain to gradually evolve as the crack passes through the material. Therefore, the transformation toughening models predict uniform remanent strain and polarization within the switching zone. Furthermore, since intermediate remanent states are not allowed within the transformation toughening model, it predicts that the out-of-plane poled material is significantly tougher than the unpoled material. Hackemann and Pfeiffer [2003] observed an increased concentration of switched domains close to the crack tip and a lower fraction of switched domains towards

the outer boundary of the switching zone. They also measured nearly identical R-curve behavior for both unpoled and out-of-plane poled material with short-circuited electrodes. The transformation toughening models cannot capture either of these observations, while the present approach does. The favorable comparison of the present model to the experimental observations suggests that ferroelectric switching behavior is more accurately modeled with an incremental plasticity formulation, rather than as an unstable phase transformation.

References

[Beom and Atluri 2003] H. G. Beom and S. N. Atluri, "Effect of electric fields on fracture behavior of ferroelectric ceramics", *J. Mech. Phys. Solids* **51**:6 (2003), 1107–1125.

[Chen and Lu 2002] Y.-H. Chen and T. J. Lu, "Cracks and fracture in piezoelectrics", *Adv. Appl. Mech.* **39** (2002), 121–215.

[Fu and Zhang 2000] R. Fu and T.-Y. Zhang, "Effects of an electric field on the fracture toughness of poled lead zirconate titanate ceramics", *J. Am. Ceram. Soc.* **83**:5 (2000), 1215–1218.

[Hackemann and Pfeiffer 2003] S. Hackemann and W. Pfeiffer, "Domain switching in process zones of PZT characterization by microdiffraction and fracture mechanical methods", *J. Eur. Ceram. Soc.* **23**:1 (2003), 141–151.

[Huber et al. 1999] J. E. Huber, N. A. Fleck, C. M. Landis, and R. M. McMeeking, "A constitutive model for ferroelectric polycrystals", *J. Mech. Phys. Solids* **47**:8 (1999), 1663–1697. MR 1686648 (2000b:74019)

[Hutchingson 1974] J. W. Hutchingson, "A course on nonlinear fracture mechanics", University Report, 1974. Harvard DEAP S-8, Division of Applied Sciences.

[Hwang and McMeeking 1998] S. C. Hwang and R. M. McMeeking, "The prediction of switching in polycrystalline ferroelectric ceramics", *Ferroelectrics* **207** (1998), 465–495.

[Kamlah 2001] M. Kamlah, "Ferroelectric and ferroelastic piezoceramics-modeling of electromechanical hysteresis phenomena", *Continuum Mech. Therm.* **13**:4 (2001), 219–268.

[Landis 2002a] C. M. Landis, "Fully coupled, multi-axial, symmetric constitutive laws for polycrystalline ferroelectric ceramics", *J. Mech. Phys. Solids* **50**:1 (2002), 127–152.

[Landis 2002b] C. M. Landis, "A new finite-element formulation for electromechanical boundary value problems", *Int. J. Numer. Methods Eng.* **55**:5 (2002), 613–628.

[Landis 2003a] C. M. Landis, "On the fracture toughness of ferroelastic materials", *J. Mech. Phys. Solids* **51**:8 (2003), 1347–1369.

[Landis 2003b] C. M. Landis, "On the strain saturation conditions for polycrystalline ferroelastic materials", *J. Appl. Mech.* (*Trans. ASME*) **70**:4 (2003), 470–478.

[Landis 2004a] C. M. Landis, "Energetically consistent boundary conditions for electromechanical fracture", *Int. J. Solids Struct.* **41**:22-23 (2004), 6291–6315.

[Landis 2004b] C. M. Landis, "In-plane complex potentials for a special class of materials with degenerate piezoelectric properties", *Int. J. Solids Struct.* **41**:3-4 (2004), 695–715.

[Landis 2004c] C. M. Landis, "Non-linear constitutive modeling of ferroelectrics", *Curr. Opin. Solid State Mater. Sci.* **8**:1 (2004), 59–69.

[Landis et al. 2000] C. M. Landis, T. Pardoen, and J. W. Hutchinson, "Crack velocity dependent toughness in rate dependent materials", *Mech. Mater.* **32**:11 (2000), 663–678.

[Landis et al. 2004] C. M. Landis, J. Wang, and J. Sheng, "Micro-electromechanical determination of the possible remanent strain and polarization states in polycrystalline ferroelectrics and the implications for phenomenological constitutive theories", *J. Intell. Mater. Syst. Struct.* **15**:7 (2004), 513–525.

[Li et al. 1985] F. Z. Li, C. F. Shih, and A. Needleman, "A comparison of methods for calculating energy release rates", *Eng. Fract. Mech.* **21**:2 (1985), 405–421.

[Lucato et al. 2002] S. L. Lucato, J. Lindner, D. C. Lupascu, and J. Rödel, "Influence of electrical and geometrical boundary conditions on crack growth in PZT", *Key Eng. Mater.* **206**:213 (2002), 609–612.

[Lynch 1996] C. S. Lynch, "The effect of uniaxial stress on the electro-mechanical response of 8/65/35 PLZT", *Acta Mater.* **44**:10 (1996), 4137–4148.

[McMeeking 1999] R. M. McMeeking, "Crack tip energy release rate for a piezoelectric compact tension specimen", *Eng. Fract. Mech.* **64**:2 (1999), 217–244.

[McMeeking and Evans 1982] R. M. McMeeking and A. G. Evans, "Mechanics of transformation toughening in brittle materials", *J. Am. Ceram. Soc.* **65**:5 (1982), 242–246.

[Park and Sun 1995] S. Park and C.-T. Sun, "Fracture criteria for piezoelectric ceramics", *J. Am. Ceram. Soc.* **78**:6 (1995), 1475–1480.

[Schneider and Heyer 1999] G. A. Schneider and V. Heyer, "Influence of the electric field on Vickers indentation crack growth in $BaTiO_3$", *J. Eur. Ceram. Soc.* **19**:6-7 (1999), 1299–1306.

[Tobin and Pak 1993] A. G. Tobin and E. Pak, "Effect of electric fields on fracture behavior of PZT ceramics", *P. Soc. Photo-Opt. Inst.* **1916** (1993), 78–86.

[Wang and Landis 2004] J. Wang and C. M. Landis, "On the fracture toughness of ferroelectric ceramics with electric field applied parallel to the crack front", *Acta Mater.* **52**:12 (2004), 3435–3446.

[Wang and Singh 1997] H. Wang and R. N. Singh, "Crack propagation in piezoelectric ceramics: effects of applied electric fields", *J. Appl. Phys.* **81**:11 (1997), 7471–7479.

[Yang and Zhu 1998] W. Yang and T. Zhu, "Switch-toughening of ferroelectrics subjected to electric fields", *J. Mech. Phys. Solids* **46**:2 (1998), 291–311.

[Zeng and Rajapakse 2001] X. Zeng and R. K. N. D. Rajapakse, "Domain switching induced fracture toughness variation in ferroelectrics", *Smart Mater. Stuct.* **10** (2001), 203–211.

[Zhang et al. 2001] T.-Y. Zhang, M. Zhao, and P. Tong, "Fracture of piezoelectric ceramics", *Adv. Appl. Mech.* **38** (2001), 147–289.

Received 5 Jan 2006.

JIANXIN WANG: wjx@rice.edu
Department of Mechanical Engineering and Materials Science, MS 321, Rice University, P.O. Box 1892, Houston, TX 77251-1892, United States

CHAD M. LANDIS: landis@rice.edu
Department of Mechanical Engineering and Materials Science, MS 321, Rice University, P.O. Box 1892, Houston, TX 77251-1892, United States
http://mems.rice.edu/~landis